Generalized Modeling of Multilink Cable-Driven Manipulators With Arbitrary Routing Using the Cable-Routing Matrix

Darwin Lau, *Member, IEEE*, Denny Oetomo, *Senior Member, IEEE*, and Saman K. Halgamuge, *Senior Member, IEEE*

***Abstract*—Multilink cable-driven manipulators offer the compactness of serial mechanisms while benefitting from the advantages of cable-actuated systems. One major challenge in modeling multilink cable-driven manipulators is that the number of combinations in the possible cable-routing increases exponentially with the number of rigid bodies. In this paper, a generalized model for multilink cable-driven serial manipulators with an arbitrary number of links that allow for arbitrary cable routing is presented. Introducing the cable-routing matrix (CRM), it is shown that all possible cable routing can be encapsulated into a single representation. The kinematics and dynamics for the generalized model are derived with respect to the CRM. The advantages of the proposed representation include the simplicity and convenience in modeling and analysis, where all cable routing is inherently considered in a single model. To illustrate this, the inverse dynamics analysis is performed for two example systems: a 2-link 4-DoF manipulator that is actuated by 6 cables and an 8-link 24-DoF mechanism actuated by 76 cables. The results show the validity and scalability of the generalized formulation, allowing for complex systems with arbitrary cable routing to be modeled and analyzed.**

***Index Terms*—Arbitrary cable routing, cable-driven manipulators, parallel mechanisms.**

I. Introduction

Cable-driven parallel manipulators have been widely studied for their desirable characteristics over serial and rigid-link parallel mechanisms: reduced end-effector weight and inertia, potentially large reachable workspace, ease of transportation, and high reconfigurability. With these advantages, a range of applications exist for cable-driven robots, including high-speed manipulators [1], [2], manufacturing [3], cargo handling [4], interaction and sensing of the environment [5], [6], building construction [7], haptics [8], [9], rehabilitation [10], [11] and exoskeletons [12].

An important characteristic of cable-driven manipulators is that cables can only actuate unilaterally through tension and not compression (*positive cable force*). An n degrees-of-freedom (DoF) system that is actuated by m cables can, therefore, be classified as being incompletely restrained if $m < n + 1$, completely restrained when $m = n + 1$, or redundantly restrained for $m > n + 1$ [13]. Completely and redundantly restrained cable-driven systems are regarded as redundantly actuated systems, resulting in challenges in the control [14]–[16], workspace analysis [17]–[21], and cable arrangement optimization [22] for this class of manipulators.

Manuscript received December 1, 2012; revised April 9, 2013; accepted May 16, 2013. Date of publication June 6, 2013; date of current version September 30, 2013. This paper was recommended for publication by Associate Editor V. Krovi and Editor B. J. Nelson upon evaluation of the reviewers' comments.

The authors are with the Department of Mechanical Engineering, The University of Melbourne, Parkville, Vic. 3010, Australia (e-mail: laudt@unimelb.edu.au; doetomo@unimelb.edu.au; saman@unimelb.edu.au).

Color versions of one or more of the figures in this paper are available online at http://ieeexplore.ieee.org.

Digital Object Identifier 10.1109/TRO.2013.2264866

Traditionally, cable-driven parallel manipulators consist of a single rigid body (*end-effector*) that is actuated by cables driven from the base frame. The design of this type of arrangement is typically not compact as the base frame is required to fully encapsulate the desired manipulator workspace. Additionally, this configuration suffers from cable-to-cable interference as the number of cables increases [23], [24]. Another class of cable-actuated manipulators is cable-driven capstan mechanisms, where the joints of the manipulator are driven by cables through capstan pulleys [25]–[28]. The advantages of this type of mechanism include its compact design and reduction of weight and inertia as the actuating motors are situated on the base platform.

A more general form of capstan mechanisms are *multilink cable-driven manipulators* [29]–[32], where the rigid bodies are actuated by cables in parallel and the cables can be arbitrarily connected through one or more of the manipulator links. This class of mechanisms benefits from the compactness of serial mechanisms, and the actuation and reconfigurability of cable-driven manipulators. Additionally, multilink cable-driven manipulators can be regarded as anthropomorphic in nature, where the rigid bodies and cables are structurally analogous to bones and muscles, respectively. Examples of previous work studied include upper-arm exoskeletons [12] and a humanoid arm [33].

The path in which a cable is connected to the links of the manipulator can be referred to as *cable routing*. Allowing for *arbitrary cable routing* results in several challenges in the modeling and analysis of this class of manipulators. First, the links of the manipulator become highly coupled as cables pass through multiple links. Furthermore, the number of possible combinations in cable routing that can exist increases exponentially as the number of links increase. The possible set of cable routing for multilink manipulators is determined through computing the permutations from the number of links. Previous studies have considered either systems with cables that are directly connected from the base to only one of the links [29] or arbitrary cable-routing systems with a relatively low number of links [30], [32].

In [29], the system dynamics for p-link open-chain manipulators were formulated using the Lagrange approach. Assuming that the cables were connected directly from the base to one of the links, only p different types of cable routing for each cable were identified and modeled. The Jacobian matrix and the wrench-closure workspace were analytically expressed for a 2-DoF 2-link planar mechanism. In [30], a 3-link 3-DoF 4-cable planar mechanism was modeled using the reciprocal screw theory. The work considered arbitrary cable routing and allowed cables to pass through multiple links. The equations of motion were generated by superimposing the reciprocal screws expressed for each link and each type of cable routing. Since each type of cable routing must be individually modeled, this approach is difficult to generalize onto systems with an increased number of links.

In this paper, a generalized model for multilink serial open-chain cable-driven spatial manipulators allowing for arbitrary cable routing is presented. The *cable-routing matrix* (*CRM*) is introduced to encapsulate all possible combinations in cable routing. Properties for the CRM are defined to ensure that the cable routing is physically meaningful. It is shown that the Jacobian matrix relating the joint and cable spaces of the manipulator can be formulated with respect to the CRM. As a result, the kinematics and dynamics for spatial multilink manipulators can be represented in a single model that allows for all possible cable routings. Inverse dynamics analysis was performed on two example systems: a 2-link 4-DoF manipulator that is actuated by 6 cables as a simple multilink system and a more complex 8-link 24-DoF system that is actuated by 76 cables.

Compared with previous work in multilink cable-driven manipulators, the proposed formulation achieves arbitrary cable routing in a generalized formulation without the need to model each individual cable routing. The proposed method can be used to model existing real-world robots, such as those from [29]–[32], providing more flexibility in the modeling of cable-routing configurations. Furthermore, the ability to model multilink cable-driven systems without assuming the number of links and cable routing is beneficial in the modeling and analysis of more complex systems. For example, biomechanical systems, such as the human limbs, neck, and spine, are serial open-chain mechanisms that typically possess a large number of rigid bodies and muscles with complex routing. Such systems can be studied as multilink cable-driven systems due to their similarities in structure and actuation.

The analysis performed on the generalized system, such as manipulator control, workspace analysis, or optimization of cable configuration, only needs to be formulated and performed once with respect to the generalized model. Additionally, rearrangement of cable routing for the system is straightforward, where only modifications to the CRM is required, as opposed to the reformulation of the system model.

The remainder of this paper is organized as follows. Section II presents the structure of the multilink manipulator model. The CRM and its properties are introduced in Section III. From the manipulator model and the CRM, the kinematics for the system are derived in Section IV. Section V formulates the system dynamics and the Jacobian matrix. The inverse dynamics analysis for the multilink model is presented in Section VI, with simulation results for two example manipulator systems.

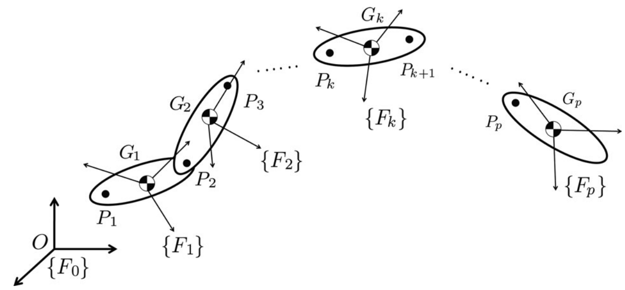

Fig. 1. Rigid body structure showing the coordinate frames, center of gravity for each link, and the joint locations.

Finally, Section VII concludes the paper and presents areas of future work.

II. Multilink Cable-Driven Manipulator Model

The model and notation for a p-link serial open-chain cable-driven system are presented in this section. Section II-A introduces the rigid body structure and Section II-B presents the model of the cables for the multilink system. The main feature of the generalized model is that it allows for any number of links and cables without any assumptions on the types of joints and cable routing.

A. Rigid Body Kinematic Structure

The model for the rigid body structure of a p-link n-DoF spatial manipulator is shown in Fig. 1. The inertial base is represented by body 0 and bodies 1 to p are the manipulator links, where link p is the outermost link. The locations G_k and P_k for $k = 1, \ldots, p$ represent the center of gravity of link k and the joint location between links k and $k-1$, respectively. The coordinate system $\{F_0\}$ represents the inertial frame with origin o_0 or O, and $\{F_k\}$ for $k = 1, \ldots, p$ corresponds to the noninertial frames that are attached to link k with origin o_k. The origin o_k is defined to be located at the center of gravity G_k.

The generalized coordinates for link k can be denoted by $\mathbf{q}_k \in \mathbb{R}^{n_k}$, where n_k is the number of DoF for link k, and define the type of joint between links k and $k-1$. For example, if links k and $k-1$ are constrained by a revolute joint with a relative angle of θ, then $n_k = 1$ and $\mathbf{q}_k = [\,\theta\,]$. If links k and $k-1$ are unconstrained, then $n_k = 6$ and the generalized coordinates can be denoted by $\mathbf{q}_k = [\,x \quad y \quad z \quad \alpha \quad \beta \quad \gamma\,]^T$, where x, y, and z represent the translation and α, β, and γ represent the orientation of link k relative to link $k-1$. The *joint space* coordinates for the entire system can be represented by $\mathbf{q} = [\,\mathbf{q}_1^T \quad \mathbf{q}_2^T \quad \ldots \quad \mathbf{q}_p^T\,]^T \in \mathbb{R}^n$, where $n = \sum_{k=1}^{p} n_k$ is the number of DoF for the system.

B. Cable Model for Multilink Systems

For the m-cable multilink cable-driven system shown in Fig. 2, the *cable space* for the system can be represented by the *cable lengths vector* $\mathbf{l} = [\,l_1 \quad l_2 \quad \ldots \quad l_m\,]^T \in \mathbb{R}^m$ and *cable forces vector* $\mathbf{f} = [\,f_1 \quad f_2 \quad \ldots \quad f_m\,]^T \in \mathbb{R}^m$, where $l_i \geq 0$

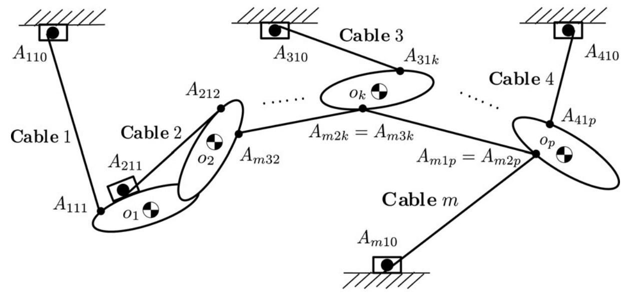

Fig. 2. Multilink cable-driven system showing the notation for the cable attachment locations. Since the system allows for arbitrary cable routing, cables may connect from base to a link (cables 1, 3, and 4), between two links (cable 2), or pass through multiple links (cable m).

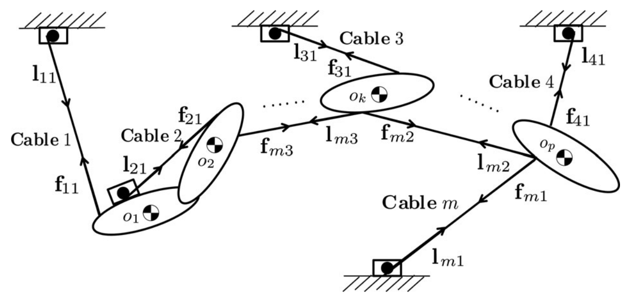

Fig. 3. Cable segment vectors showing the relationship between the cable vector $\mathbf{l}_{ij}$ and force vector $\mathbf{f}_{ij}$.

and $f_i \geq 0$ represent the length and tension force of cable i, respectively.

Allowing cables to pass through multiple links, each cable consists of multiple *cable segments*, where a cable segment is defined as the section of the cable between two bodies. To ensure that the cable routing is physically realizable, Assumption 1 ensures that cables have a finite number of cable segments.

Assumption 1: Each cable must have a finite number of cable segments, where s_i is the number of segments for cable i.

Hence, the maximum number of segments that a cable can possess in the system is $s = \max_i s_i$. The attachment point of segment j of cable i on link k, as shown in Fig. 2, can be denoted by A_{ijk}. The kinematics of a cable with multiple segments can be described by *cable segment vectors*, where the cable segment vector for segment j of cable i, as shown in Fig. 3, can be denoted by $\mathbf{l}_{ij}$.

If segment j of cable i is attached from link a to link b, the corresponding cable segment vector can be defined as

$$\mathbf{l}_{ij} = -\mathbf{r}_{OA_{ija}} + \mathbf{r}_{OA_{ijb}} \; \forall j \in \{1, \ldots, s_i\}. \tag{1}$$

Denoting the length of segment j of cable i as $l_{ij} = ||\mathbf{l}_{ij}||$, the length of cable i can be expressed as

$$l_i = \sum_{j=1}^{s_i} l_{ij}. \tag{2}$$

For the remaining segments $j > s_i$, the cable segment vector $\mathbf{l}_{ij}$ can be assumed to be a zero vector, where

$$\mathbf{l}_{ij} = \mathbf{0} \;\; \forall j > s_i. \tag{3}$$

Hence, from (2) and (3), the length of the cable i can be equivalently expressed as

$$l_i = \sum_{j=1}^{s} l_{ij}. \tag{4}$$

Similarly, the forces for a cable with multiple segments can be described by *cable segment force vectors*, where the cable segment force vector for segment j of cable i can be denoted by $\mathbf{f}_{ij}$. Assuming that the segments of a cable route through a frictionless pulley, the force in a cable can be assumed to be uniform across all its segments. Hence, from Fig. 3, it can be observed that $\mathbf{f}_{ij}$ can be related to $\mathbf{l}_{ij}$ by

$$\mathbf{f}_{ij} = -\hat{\mathbf{l}}_{ij} f_i \; \forall j \tag{5}$$

where $\hat{\mathbf{l}}_{ij}$ is the unit vector of $\mathbf{l}_{ij}$.

III. Cable-Routing Matrix

To represent the cable routing for multilink cable-driven systems, a *CRM* is introduced. Each term $c_{ij(k+1)}$ within the CRM describes the cable-routing relationship between segment j of cable i and link k, where

1) $c_{ij(k+1)} = -1$ denotes that segment j of cable i begins from link k;
2) $c_{ij(k+1)} = 1$ denotes that segment j of cable i ends at link k;
3) $c_{ij(k+1)} = 0$ denotes that segment j of cable i is not connected to link k.

For an m-cable system, each cable has a maximum of s segments and each cable segment can be attached onto $p + 1$ bodies (inertial base frame and p system links). Defining $\mathcal{C} = \{-1, 0, 1\}$, the CRM for a system C can be regarded as a 3-D matrix with dimensions $m \times s \times (p + 1)$ and $C \in \mathcal{C}^{m \times s \times (p+1)}$. The cable routing for each cable can be extracted from the CRM and represented by a set of matrices $C_1, C_2, \ldots, C_m \in \mathcal{C}^{s \times (p+1)}$, where C_i is a $s \times (p + 1)$ matrix that describes the cable routing for cable i. Row j of C_i represents the cable routing for segment j of cable i and element (j, k) of C_i represents the term c_{ijk} within the CRM.

The CRM can be regarded as the descriptor of the cable routing for generalized multilink cable-driven manipulators, where all possible cable routings are encapsulated within a single matrix representation. The kinematics and dynamics of the system can then be modeled with respect to the CRM, resulting in a generalized model without predefining the cable routing for the system. Furthermore, the result of any analysis that is performed on the generalized model, such as inverse dynamics, control, workspace analysis, and cable configuration optimization, can be described with respect to the CRM. The primary advantage of the CRM is that the modeling and analysis is only required to be performed once on the generalized model, and any reconfiguration of the cable routing only requires modification to the elements of the CRM.

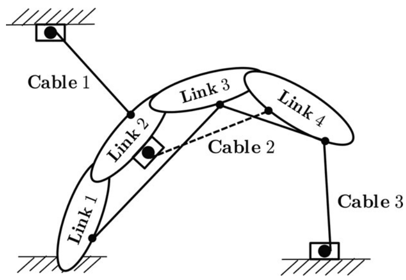

Fig. 4. Simple 4-link 3-cable example system to demonstrate how the CRM can be used to describe different types of cable routing.

A. Cable-Routing Matrix Example

For the 4-link 3-cable manipulator shown in Fig. 4, the CRM will be formulated to illustrate how the routing of cables and segments can be defined. Without the loss of generality, the maximum number of segments can be set as $s = 4$. Hence, each cable can have a maximum of four segments and can be attached to 5 bodies: the inertial base and links 1 through to 4. The resulting CRM can be denoted as $C \in \mathcal{C}^{3\times 4\times 5}$, and matrices $C_1, C_2, C_3 \in \mathcal{C}^{4\times 5}$ describes the cable routing for cables 1, 2, and 3, respectively.

From Fig. 4, cable 1 is connected from the base platform to link 2, and can be described by

$$C_1 = \begin{bmatrix} -1 & 0 & 1 & 0 & 0 \\ 0 & 0 & 0 & 0 & 0 \\ 0 & 0 & 0 & 0 & 0 \\ 0 & 0 & 0 & 0 & 0 \end{bmatrix}.$$

Cable 1 only consists of a single segment, corresponding to the first row in C_1 and $c_{1jk} = 0 \; \forall j > 1$. Segment 1 begins from the base and ends at link 2, represented by $c_{111} = -1$ and $c_{113} = 1$, respectively. Similarly, the routing matrix for cable 2 is represented by

$$C_2 = \begin{bmatrix} 0 & 0 & -1 & 0 & 1 \\ 0 & 0 & 0 & 0 & 0 \\ 0 & 0 & 0 & 0 & 0 \\ 0 & 0 & 0 & 0 & 0 \end{bmatrix}.$$

Cable 2 consists of a single segment, hence $c_{2jk} = 0 \; \forall j > 1$, and begins from link 2 and ends at link 4, represented by $c_{213} = -1$ and $c_{215} = 1$, respectively. Considering a multisegment example, the routing matrix for cable 3 is represented by

$$C_3 = \begin{bmatrix} -1 & 0 & 0 & 0 & 1 \\ 0 & 0 & 0 & 1 & -1 \\ 0 & 1 & 0 & -1 & 0 \\ 0 & 0 & 0 & 0 & 0 \end{bmatrix}.$$

From C_3, cable 3 consists of three segments, where the first segment begins from the base and ends at link 4, represented by the first row of C_3 where $c_{311} = -1$ and $c_{315} = 1$, respectively. The second row of C_3 defines that the second segment begins at link 4 and ends at link 3, represented by $c_{325} = -1$ and $c_{324} = 1$, respectively. Finally, segment 3 begins at link 3 and ends at link 1, represented by $c_{334} = -1$ and $c_{332} = 1$, respectively.

B. Cable-Routing Matrix Properties

To ensure that the cable routing of a system is feasible and physically meaningful, a set of properties for the CRM that represent the necessary and sufficient conditions on valid cable routing are defined. Properties on the CRM can be utilized in verifying the validity of CRMs and in constructing feasible cable routing. The construction of feasible CRMs is important in automating the design process of cable-driven multilink mechanisms.

Properties 1 and 2 ensure that every cable segment $j \leq s_i$ is feasible, where each segment has exactly one beginning and one ending attachment. Property 3 ensures that the remaining segments $j > s_i$ are not attached onto any links and that $\mathbf{l}_{ij} = \mathbf{0} \; \forall j > s_i$ from (3) is satisfied.

Property 1: $\sum_{k=1}^{p+1} c_{ijk} = 0 \; \forall i \in \{1, \ldots, m\} \; \forall j \in \{1, \ldots, s\}$. Every cable segment must have an equal number of beginning and ending attachments.

Property 2: $\sum_{k=1}^{p+1} |c_{ijk}| = 2 \, \forall i \in \{1, \ldots, m\} \; \forall j \in \{1, \ldots, s_i\}$. Each segment from 1 to s_i must be attached to two different links, where $1 \leq s_i \leq s$ is the total number of segments for cable i.

Property 3: $c_{ijk} = 0 \; \forall i \in \{1, \ldots, m\} \; \forall j \in \{s_i + 1, \ldots, s\} \; \forall k \in \{1, \ldots, p + 1\}$. Following from Property 2, the remaining virtual segments $j > s_i$ must not have any attachment points to any links.

Property 4 ensures that for cables with multiple segments, the ending attachment of a segment and the beginning attachment of the next segment are connected at the same location.

Property 4: $\forall i \in \{1, \ldots, m\} \; \forall j \in \{1, \ldots, s_i - 1\} \exists k \in \{1, \ldots, p + 1\} : c_{ijk} - c_{i(j+1)k} = 2$. Combining with Properties 1 and 2, consecutive segments are connected such that the ending attachment of segment j and beginning attachment of segment $j + 1$ are attached onto the same link.

As a result of Property 4, the CRM is structured such that rows 1 and s_i of C_i represent the first and last segments of cable i. Hence, if cable i begins on link a, then $c_{i1(a+1)} = -1$ and location A_{i1a} can be regarded as the *beginning attachment point* for cable i. Similarly, if cable i ends on link b, then $c_{is_i(b+1)} = 1$ and location A_{is_ib} can be regarded as the *ending attachment point* for cable i. From the aforementioned properties, each cable must have one beginning and one ending attachment point. For cables with multiple segments, the connection locations between consecutive segments can be regarded as *pass-through attachment points*.

Properties 1 to 4 represent a minimum set of properties for any multilink cable-driven system such that the cables and its segments defined by the CRM are valid. In a similar manner to the proposed properties, additional properties can be defined to impose constraints on how the cables attach or pass through the links of the manipulator depending on the specific requirements for the manipulator. For example, requiring that each cable only be attached to each link of the manipulator at most one can ensure that the cables do not form closed loops. To satisfy this requirement, Properties 5 and 6 can be defined on the CRM.

Property 5: $\sum_{k=1}^{p+1} |\sum_j c_{ijk}| = 2\,\forall i$. The beginning attachment point and ending attachment point of every cable are located at different links. If the beginning or ending attachment point of cable i is located at link $k-1$, then $\sum_j c_{ijk} = -1$ or $\sum_j c_{ijk} = 1$, respectively. Otherwise, if cable i does not attach onto or pass through link $k-1$, then $\sum_j c_{ijk} = 0$. If the beginning and ending attachments of cable i are on the same link, then $\sum_k |\sum_j c_{ijk}| = 0$ and the cable forms a closed loop.

Property 6: $\sum_j |c_{ijk}| \leq 2\,\forall i\,\forall k$. Following from Property 5, cable i is connected to link $k-1$ at most once. Cable i is either not connected to link $k-1$ ($\sum_j |c_{ijk}| = 0$), begins or ends on link $k-1$ ($\sum_j |c_{ijk}| = 1$), or passes through link $k-1$ ($\sum_j |c_{ijk}| = 2$).

IV. Kinematics

In this section, the direct kinematics and Jacobian matrix J with respect to the CRM will be derived. The Jacobian matrix represents the kinematic relationship between the time derivative of cable lengths $\dot{\mathbf{l}}$ and the time derivative of joint space coordinates $\dot{\mathbf{q}}$, where $\dot{\mathbf{l}} = J\dot{\mathbf{q}}$. From the definition of the CRM presented in Section III, the cable segment vector from (1) can be expressed as

$$\mathbf{l}_{ij} = \sum_{k=0}^{p} \left[c_{ij(k+1)} \mathbf{r}_{OA_{ijk}} \right]. \tag{6}$$

The length of cable i can be determined by substituting the cable segment vector from (6) into (4), where

$$l_i = \sum_{j=1}^{s} \left\| \sum_{k=0}^{p} c_{ij(k+1)} \mathbf{r}_{OA_{ijk}} \right\|. \tag{7}$$

The relationship from (7) represents the direct kinematics for the generalized multilink cable-driven system.

To relate $\dot{\mathbf{l}}$ and $\dot{\mathbf{q}}$, the manipulator *task space* $\mathbf{x}$ is introduced. The time derivative of the task space $\dot{\mathbf{x}}$ represents the absolute linear velocities of the center of mass and absolute angular velocities for each body of the system, where

$$\dot{\mathbf{x}} = \begin{bmatrix} {}^1\dot{\mathbf{r}}_{O_{o_1}}^T & {}^1\boldsymbol{\omega}_1^T & \dots & {}^p\dot{\mathbf{r}}_{O_{o_p}}^T & {}^p\boldsymbol{\omega}_p^T \end{bmatrix}^T.$$

Vectors ${}^k\dot{\mathbf{r}}_{O_{o_k}}$ and ${}^k\boldsymbol{\omega}_k$ refer to the absolute linear velocity of point o_k and absolute angular velocity of body k, respectively. The left superscript k denotes that the vector is expressed in $\{F_k\}$. The time derivative of the length of segment j of cable i can be determined by

$$\dot{l}_{ij} = \hat{\mathbf{l}}_{ij} \cdot \dot{\mathbf{l}}_{ij}. \tag{8}$$

Substituting (8) and time derivative of (6) into the time derivative of (4) allows $\dot{l}_i$ to be expressed with respect to the CRM, where

$$\begin{aligned} \dot{l}_i &= \sum_{j=1}^{s} \dot{l}_{ij} \\ &= \sum_{j=1}^{s} \sum_{k=0}^{p} \left[c_{ij(k+1)} {}^k\hat{\mathbf{l}}_{ij} \cdot {}^k\dot{\mathbf{r}}_{OA_{ijk}} \right]. \end{aligned} \tag{9}$$

Since ${}^0\dot{\mathbf{r}}_{OA_{ij0}} = \mathbf{0}$ as ${}^0\mathbf{r}_{OA_{ij0}}$ is fixed in $\{F_0\}$, and ${}^k\dot{\mathbf{r}}_{OA_{ijk}} = {}^k\dot{\mathbf{r}}_{O_{o_k}} + {}^k\boldsymbol{\omega}_k \times {}^k\mathbf{r}_{o_kA_{ijk}}$, then (9) can be expressed in the form

$$\begin{aligned} \dot{l}_i &= \sum_{k=1}^{p} \sum_{j=1}^{s} \left[c_{ij(k+1)} {}^k\hat{\mathbf{l}}_{ij} \cdot \left({}^k\dot{\mathbf{r}}_{O_{o_k}} + {}^k\boldsymbol{\omega}_k \times {}^k\mathbf{r}_{o_kA_{ijk}} \right) \right] \\ &= \sum_{k=1}^{p} \left[V_{i\mathbf{x}_k} \dot{\mathbf{r}}_{O_{o_k}} + V_{i\boldsymbol{\theta}_k} \boldsymbol{\omega}_k \right] \end{aligned} \tag{10}$$

where

$$\begin{aligned} V_{i\mathbf{x}_k} &= \left(\sum_{j=1}^{s} \left[c_{ij(k+1)} {}^k\hat{\mathbf{l}}_{ij} \right] \right)^T \\ V_{i\boldsymbol{\theta}_k} &= \left(\sum_{j=1}^{s} \left[c_{ij(k+1)} {}^k\mathbf{r}_{o_kA_{ijk}} \times {}^k\hat{\mathbf{l}}_{ij} \right] \right)^T. \end{aligned} \tag{11}$$

The terms $V_{i\mathbf{x}_k}$ and $V_{i\boldsymbol{\theta}_k}$ represent the relationship between the task space velocities of link k and the time derivative of the length of cable i. From (10), the relationship between $\dot{\mathbf{l}}$ and $\dot{\mathbf{x}}$ can be expressed in the form $\dot{\mathbf{l}} = V\dot{\mathbf{x}}$, where

$$V = \begin{bmatrix} V_{1\mathbf{x}_1} & V_{1\boldsymbol{\theta}_1} & \dots & V_{1\mathbf{x}_p} & V_{1\boldsymbol{\theta}_p} \\ \vdots & & & & \vdots \\ V_{m\mathbf{x}_1} & V_{m\boldsymbol{\theta}_1} & \dots & V_{m\mathbf{x}_p} & V_{m\boldsymbol{\theta}_p} \end{bmatrix} \in \mathbb{R}^{m\times 6p}. \tag{12}$$

The relationship between the time derivative of the joint space coordinates $\dot{\mathbf{q}}$ and task space velocities $\dot{\mathbf{x}}$ can be determined from the expressions of absolute linear and angular velocities of link k in $\{F_k\}$, where

$$\begin{aligned} {}^k\dot{\mathbf{r}}_{O_{o_k}} &= \sum_{a=1}^{k} \left[W_{a\mathbf{x}_k} \dot{\mathbf{q}}_a \right] \\ {}^k\boldsymbol{\omega}_k &= \sum_{a=1}^{k} \left[W_{a\boldsymbol{\theta}_k} \dot{\mathbf{q}}_a \right]. \end{aligned} \tag{13}$$

The terms $W_{a\mathbf{x}_k}$ and $W_{a\boldsymbol{\theta}_k}$ represent the linear relationship between $\dot{\mathbf{q}}_a$ and the relative linear and angular velocities, respectively, between links k and $k-1$. The relationship (13) can be expressed for the entire system in the form $\dot{\mathbf{x}} = W\dot{\mathbf{q}}$, where

$$W = \begin{bmatrix} W_{1\mathbf{x}_1} & 0_{1\times n_2} & \dots & 0_{1\times n_p} \\ W_{1\boldsymbol{\theta}_1} & 0_{1\times n_2} & \dots & 0_{1\times n_p} \\ \vdots & & & \vdots \\ W_{1\mathbf{x}_p} & W_{2\mathbf{x}_p} & \dots & W_{p\mathbf{x}_p} \\ W_{1\boldsymbol{\theta}_p} & W_{2\boldsymbol{\theta}_p} & \dots & W_{p\boldsymbol{\theta}_p} \end{bmatrix} \in \mathbb{R}^{6p\times n}. \tag{14}$$

From (12) and (14), the relationship between the time derivative of the cable length vector and time derivative of the joint space coordinates can be expressed as $\dot{\mathbf{l}} = VW\dot{\mathbf{q}} = J\dot{\mathbf{q}}$, where J is the Jacobian matrix of the system. The Jacobian matrix can be expressed as

$$J = \begin{bmatrix} J_{11} & J_{12} & \dots & J_{1p} \\ \vdots & & & \vdots \\ J_{m1} & J_{m2} & \dots & J_{mp} \end{bmatrix} \in \mathbb{R}^{m \times n} \tag{15}$$

where

$$J_{ia} = \sum_{k=a}^{p} \left[V_{i\mathbf{x}_k} W_{a\mathbf{x}_k} + V_{i\boldsymbol{\theta}_k} W_{a\boldsymbol{\theta}_k} \right]. \tag{16}$$

The Jacobian matrix term $J_{ia} \in \mathbb{R}^{1 \times n_a}$ represents the relationship between the time derivative of the length of cable i and the time derivative of the joint space coordinates of link a. The Jacobian matrix from (15) for the generalized system encapsulates all possible cable routing as terms $V_{i\mathbf{x}_k}$ and $V_{i\boldsymbol{\theta}_k}$ from (11) are generically defined with respect to the CRM terms.

V. Dynamics

The equations of motion for the generalized multilink system can be expressed in the form

$$M(\mathbf{q})\ddot{\mathbf{q}} + \mathbf{C}(\mathbf{q}, \dot{\mathbf{q}}) + \mathbf{G}(\mathbf{q}) + \boldsymbol{\Gamma}_e = -J^T(\mathbf{q})\mathbf{f} \tag{17}$$

where $M, \mathbf{C}, \mathbf{G}$, and $\boldsymbol{\Gamma}_e$ represent the mass-inertia matrix, centrifugal and Coriolis vector, gravitational vector, and external force vector, respectively.

The force and moment acting on link k due to cable i can be denoted as $\mathbf{F}_{T_{ik}}$ and $\mathbf{M}_{T_{ik}}$, respectively. Utilizing (5), the force and moment can be expressed as

$$\begin{aligned} {}^k\mathbf{F}_{T_{ik}} &= \sum_{j=1}^{s} \left[c_{ij(k+1)} {}^k\mathbf{f}_{ij} \right] \\ &= -\sum_{j=1}^{s} \left[c_{ij(k+1)} {}^k\hat{\mathbf{l}}_{ij} \right] f_i \\ {}^k\mathbf{M}_{T_{ik}} &= -\sum_{j=1}^{s} \left[c_{ij(k+1)} {}^k\mathbf{r}_{o_k A_{ijk}} \times {}^k\hat{\mathbf{l}}_{ij} \right] f_i \end{aligned} \tag{18}$$

where moments are evaluated about the link's center of gravity o_k. The CRM element $c_{ij(k+1)}$ from (18) represents the relationship between the force of segment j of cable i and link k. For example, $c_{ij(k+1)} = 0$ indicates that the force of the cable segment does not produce a resultant force or moment on the link. Summing the forces and moments from (18) across all cables, the resultant force and moment acting on link k due to the cable forces can be expressed as

$$\begin{aligned} {}^k\mathbf{F}_{T_k} &= -\sum_{i=1}^{m} \left[V_{i\mathbf{x}_k}^T f_i \right] \\ {}^k\mathbf{M}_{T_k} &= -\sum_{i=1}^{m} \left[V_{i\boldsymbol{\theta}_k}^T f_i \right] \end{aligned} \tag{19}$$

where $V_{i\mathbf{x}_k}^T$ and $V_{i\boldsymbol{\theta}_k}^T$ are the transpose of the terms from (11) and represent the relationship between the force in cable i and the resultant wrench on link k. From (19), the resultant wrench on the entire system due to the cable forces vector can be expressed with respect to (12) as

$$\mathbf{w}_T = -V^T\mathbf{f} \tag{20}$$

where $\mathbf{w}_T = \left[{}^1\mathbf{F}_{T_1}^T \quad {}^1\mathbf{M}_{T_1}^T \quad \dots \quad {}^p\mathbf{F}_{T_p}^T \quad {}^p\mathbf{M}_{T_p}^T \right]^T$. The equations of motion for the system can be determined by propagating the dynamics of each individual body and projecting the forces onto the system joint space. The dynamics for link k can be expressed in $\{F_k\}$ as

$$\begin{aligned} \frac{d}{dt}\left(m_k {}^k\dot{\mathbf{r}}_{OG_k} \right) &= {}^k\mathbf{F}_{T_k} + {}^k\mathbf{F}_{R_k} + {}^k\mathbf{F}_{E_k} + {}^k\mathbf{G}_k \\ \frac{d}{dt}\left(I_k {}^k\boldsymbol{\omega}_k \right) &= {}^k\mathbf{M}_{T_k} + {}^k\mathbf{M}_{R_k} + {}^k\mathbf{M}_{E_k} \end{aligned} \tag{21}$$

where m_k and I_k are the mass and inertia matrix of link k, respectively. The resultant force and moment acting on body k are comprised of cable wrench $\mathbf{F}_{T_k}$ and $\mathbf{M}_{T_k}$, total interaction force $\mathbf{F}_{R_k}$ and moment $\mathbf{M}_{R_k}$, external wrenches $\mathbf{F}_{E_k}$ and $\mathbf{M}_{E_k}$, and gravity force $\mathbf{G}_k$. For a serial manipulator, the total interaction force and moment on link k comprises the interaction forces and moments at joints P_k and P_{k+1}, as shown in Fig. 1, and can be expressed as

$$\begin{aligned} {}^k\mathbf{F}_{R_k} &= {}^k\mathbf{F}_{P_k} - {}^k\mathbf{F}_{P_{k+1}} \\ {}^k\mathbf{M}_{R_k} &= {}^k\mathbf{M}_{P_k} + {}^k\mathbf{r}_{G_k P_k} \times {}^k\mathbf{F}_{P_k} - {}^k\mathbf{M}_{P_{k+1}} \\ &\quad - {}^k\mathbf{r}_{G_k P_{k+1}} \times {}^k\mathbf{F}_{P_{k+1}} \end{aligned} \tag{22}$$

where $\mathbf{F}_{P_k}$ and $\mathbf{M}_{P_k}$ are the interaction force and moment at joint P_k, respectively.

The equations of motion for link a can be derived by projecting the interaction forces and moments at P_a onto the directions of the nonworking interaction forces. The projection results in the relationship

$$S_a^T \begin{bmatrix} {}^a\mathbf{F}_{P_a} \\ {}^a\mathbf{M}_{P_a} \end{bmatrix} = 0_{n_a \times 1} \tag{23}$$

where $S_a^T \in \mathbb{R}^{n_a \times 6}$ represents the projection of interaction force and moment onto the generalized coordinates of link a. Beginning from the outermost link, $\mathbf{F}_{P_{p+1}} = \mathbf{M}_{P_{p+1}} = \mathbf{0}$, and the interaction force and moment at P_p can be determined from (21) and (22) as

$$\begin{aligned} {}^p\mathbf{F}_{P_p} &= {}^p\mathbf{F}_p^* \\ {}^p\mathbf{M}_{P_p} &= {}^p\mathbf{M}_p^* + {}^p\mathbf{r}_{P_p G_p} \times {}^p\mathbf{F}_p^* \end{aligned} \tag{24}$$

where $\mathbf{F}_k^*$ and $\mathbf{M}_k^*$ can be expressed as

$$\begin{aligned} {}^k\mathbf{F}_k^* &= \frac{d}{dt}\left(m_k \dot{\mathbf{r}}_{OG_k} \right) - \mathbf{F}_{T_k} - \mathbf{F}_{E_k} - \mathbf{G}_k \\ {}^k\mathbf{M}_k^* &= \frac{d}{dt}\left(I_k \boldsymbol{\omega}_k \right) - \mathbf{M}_{T_k} - \mathbf{M}_{E_k}. \end{aligned} \tag{25}$$

Similarly, the interaction force and moment at joint P_{p-1} are

$$\begin{aligned} {}^{p-1}\mathbf{F}_{P_{p-1}} &= \mathbf{F}_{p-1}^* + {}_p^{p-1}R^p\mathbf{F}_{P_p} \\ &= \mathbf{F}_{p-1}^* + {}_p^{p-1}R\,\mathbf{F}_p^* \\ {}^{p-1}\mathbf{M}_{P_{p-1}} &= \mathbf{M}_{p-1}^* + \mathbf{r}_{P_{p-1}G_{p-1}} \times \mathbf{F}_{P_{p-1}} \end{aligned}$$

$$+ {}^{p-1}_{p}R\,\mathbf{M}_{P_p} + \mathbf{r}_{G_{p-1}P_p} \times \left({}^{p-1}_{p}R\,\mathbf{F}_{P_p}\right)$$
$$= \mathbf{M}^*_{p-1} + {}^{p-1}_{p}R\,\mathbf{M}^*_p + \mathbf{r}_{P_{p-1}G_{p-1}} \times \mathbf{F}^*_{p-1}$$
$$+ \mathbf{r}_{P_{p-1}G_p} \times \left({}^{p-1}_{p}R\,\mathbf{F}^*_p\right). \quad (26)$$

Generalizing the interaction force and moment relationships from (24) and (26), the interaction force and moment at joint P_a can be expressed as

$$\begin{aligned} {}^{a}\mathbf{F}_{P_a} &= \sum_{k=a}^{p} \left[{}^{a}_{k}R\,\mathbf{F}^*_k\right] \\ {}^{a}\mathbf{M}_{P_a} &= \sum_{k=a}^{p} \left[{}^{a}_{k}R\,\mathbf{M}^*_k + {}^{a}\mathbf{r}_{P_aG_k} \times \left({}^{a}_{p}R\,\mathbf{F}^*_k\right)\right]. \end{aligned} \quad (27)$$

Substituting (27) into (23), the equations of motion for link a can be expressed as

$$S_a^T \sum_{k=a}^{p} \left[\begin{bmatrix} {}^{a}_{k}R \\ \left[{}^{a}\mathbf{r}_{P_aG_k}\right]^{\times a}_{\;\;k}R \end{bmatrix} \mathbf{F}^*_k + \begin{bmatrix} 0 \\ {}^{a}_{k}R \end{bmatrix} \mathbf{M}^*_k\right] = \mathbf{0}. \quad (28)$$

The terms $W^T_{a\mathbf{x}_k}$ and $W^T_{a\boldsymbol{\theta}_k}$ are the transpose of $W_{a\mathbf{x}_k}$ and $W_{a\boldsymbol{\theta}_k}$ from (13), respectively. For serial manipulators, the terms can be defined as

$$\begin{aligned} W^T_{a\mathbf{x}_k} &= S_a^T \begin{bmatrix} {}^{a}_{k}R \\ \left[{}^{a}\mathbf{r}_{P_aG_k}\right]^{\times a}_{\;\;k}R \end{bmatrix} \\ W^T_{a\boldsymbol{\theta}_k} &= S_a^T \begin{bmatrix} 0 \\ {}^{a}_{k}R \end{bmatrix}. \end{aligned} \quad (29)$$

Substituting (29) into (28) results in

$$\sum_{k=a}^{p} \left[W^T_{a\mathbf{x}_k}\mathbf{F}^*_k + W^T_{a\boldsymbol{\theta}_k}\mathbf{M}^*_k\right] = \mathbf{0}. \quad (30)$$

The equations of motion for the system can be determined by incorporating (25) into (30) for each body, resulting in

$$W^T \begin{bmatrix} m_1\ddot{\mathbf{r}}_{OG_1} - \mathbf{G}_1 - \mathbf{F}_{E_1} \\ \dfrac{d}{dt}(I_1\boldsymbol{\omega}_1) - \mathbf{M}_{E_1} \\ \vdots \\ m_p\ddot{\mathbf{r}}_{OG_p} - \mathbf{G}_p - \mathbf{F}_{E_p} \\ \dfrac{d}{dt}(I_p\boldsymbol{\omega}_p) - \mathbf{M}_{E_p} \end{bmatrix} = W^T \begin{bmatrix} \mathbf{F}_{T_1} \\ \mathbf{M}_{T_1} \\ \vdots \\ \mathbf{F}_{T_p} \\ \mathbf{M}_{T_p} \end{bmatrix}. \quad (31)$$

From (20), the relationship between the cable forces and generalized forces on the manipulator can be expressed as

$$W^T\mathbf{w}_T = -W^TV^T\mathbf{f} = -J^T\mathbf{f}. \quad (32)$$

It can be observed that the substitution of (32) into (31) results in the equations of motion of the general form (17), where J^T is the transpose of the Jacobian matrix from (15), where

$$J^T = \begin{bmatrix} J^T_{11} & J^T_{21} & \dots & J^T_{m1} \\ \vdots & & & \vdots \\ J^T_{1p} & J^T_{2p} & \dots & J^T_{mp} \end{bmatrix} \in \mathbb{R}^{n\times m}. \quad (33)$$

The transpose of the Jacobian matrix term J^T_{ia} can be expressed as

$$J^T_{ia} = \sum_{k=a}^{p} \left[W^T_{a\mathbf{x}_k}V^T_{i\mathbf{x}_k} + W^T_{a\boldsymbol{\theta}_k}V^T_{i\boldsymbol{\theta}_k}\right]. \quad (34)$$

The definition of the transpose of the Jacobian matrix and its terms from (33) and (34), respectively, is consistent with the Jacobian matrix and its terms from (15) and (16), respectively. The term $J^T_{ia} \in \mathbb{R}^{n_a\times 1}$ represents the relationship between the force of cable i and the generalized force of link a.

VI. Inverse Dynamics Analysis

The inverse dynamics problem for cable-driven manipulators refers to the determination of positive cable forces to achieve a desired trajectory described with respect to the generalized coordinates $\mathbf{q}_r(t)$, $\dot{\mathbf{q}}_r(t)$, and $\ddot{\mathbf{q}}_r(t)$. The actuation redundancy in cable-driven systems is typically resolved by optimizing for an objective function expressed as a function of the cable forces. The inverse dynamics problem at time t can be defined as

$$\begin{aligned} &\mathbf{f}^* = \arg\min_{\mathbf{f}} Q(\mathbf{f}) \\ &\text{s.t} \quad M(\mathbf{q}_r)\ddot{\mathbf{q}}_r + \mathbf{C}(\mathbf{q}_r, \dot{\mathbf{q}}_r) + \mathbf{G}(\mathbf{q}_r) + \boldsymbol{\Gamma}_e = -J^T(\mathbf{q}_r)\mathbf{f} \\ &\qquad \mathbf{0} \le \mathbf{f}_{\min} \le \mathbf{f} \le \mathbf{f}_{\max} \end{aligned} \quad (35)$$

where $\mathbf{f}^*$ is the resolved cable forces through the minimization of the objective function $Q(\mathbf{f})$. The minimum and maximum bounds on the cable forces are denoted by $\mathbf{f}_{\min}$ and $\mathbf{f}_{\max}$, respectively. Common objective functions include linear and quadratic functions, $Q_1(\mathbf{f}) = H_1\mathbf{f}$ and $Q_2(\mathbf{f}) = \mathbf{f}^TH_2\mathbf{f} + H_3\mathbf{f}$, respectively, where $H_1 \in \mathbb{R}^{1\times m}$, $H_2 \in \mathbb{R}^{m\times m}$, and $H_3 \in \mathbb{R}^{1\times m}$ represent weightings for the distribution of cable forces [15], [34]. Since both constraints in (35) are linear, the class of the optimization problem depends on the objective function. For example, selection of $Q(\mathbf{f}) = Q_1(\mathbf{f})$ or $Q(\mathbf{f}) = Q_2(\mathbf{f})$ results in a linear programming or quadratic programming problem, respectively. The quadratic function $Q(\mathbf{f}) = \mathbf{f}^T\mathbf{f}$ will be utilized for the examples in this section. Without the loss of generality, the cable routing for the examples in this section do not form closed loops, and hence the maximum number of segments is defined as $s = p$ for a p-link system.

A. 2-Link 4-Degree of Freedom Spherical-Revolute System

A 2-link spatial manipulator with 4 DoF is shown in Fig. 5. Link 1 is constrained to origin of the inertial frame through a spherical (S) joint, and links 2 and 1 are constrained by a revolute (R) joint. The generalized coordinates for the system can be expressed by $\mathbf{q} = [\alpha \quad \beta \quad \gamma \quad \theta]^T$, where α, β, and γ represent the xyz-Euler angles of the spherical joint and θ represents the relative angle of the revolute joint.

The system is actuated by 6 cables, where cables 1 to 4 are connected from the base to link 1, and cables 5 and 6 are connected from the base to link 2, passing via link 1. The CRMs

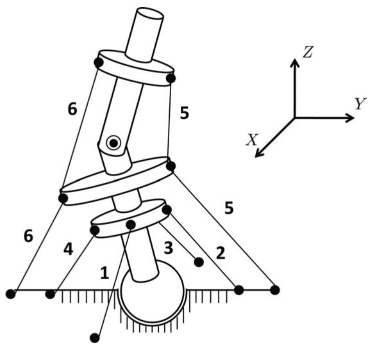

Fig. 5. 2-link Spherical-Revolute 6-cable model.

for cables 1 to 4, denoted by C_1 to C_4, respectively, are

$$C_1 = C_2 = C_3 = C_4 = \begin{bmatrix} -1 & 1 & 0 \\ 0 & 0 & 0 \end{bmatrix}$$

and the CRMs for cables 5 and 6 can be expressed by

$$C_5 = C_6 = \begin{bmatrix} -1 & 1 & 0 \\ 0 & -1 & 1 \end{bmatrix}.$$

In this system, the attachment locations of the cables $\mathbf{r}_{O_k A_{ijk}}$ are symmetrically arranged, such that when the manipulator is in its zero upright position, cables 1 and 3 are located in the XZ-plane, and the remaining cables are located in the YZ-plane.

A simple trajectory was selected to demonstrate the inverse dynamics of the generalized equations of motion for the 2-link system. The desired trajectory $\mathbf{q}_r(t)$ was constructed by interpolating from the initial pose $\mathbf{q}_s = [\,\frac{\pi}{10} \quad 0 \quad 0 \quad -\frac{\pi}{6}\,]^T$ to the final pose $\mathbf{q}_e = [\,-\frac{\pi}{10} \quad 0 \quad 0 \quad \frac{\pi}{6}\,]^T$. Additionally, the initial and final velocities and accelerations for the desired trajectory were set to zero $\dot{\mathbf{q}}_s = \dot{\mathbf{q}}_e = \ddot{\mathbf{q}}_s = \ddot{\mathbf{q}}_e = \mathbf{0}$. Fig. 5 shows the manipulator in its initial pose $\mathbf{q}_s$.

Fig. 6 shows the resulting cable forces that are required to produce the desired trajectory $\mathbf{q}_r(t)$. The minimum and maximum bounds on cable forces were set to 0.001N and 1000 N, respectively. Since the motion $\mathbf{q}_r(t)$ is purely in the YZ-plane, it is expected that cables 1 and 3 both exert the minimum tension value, as shown in Fig. 6(a) and (c), respectively. For the motion $t \le 0.5$ s, cables 2 and 6 are required to actuate the motion of links 1 and 2, respectively. Since cable 6 is connected to both links 1 and 2, it causes link 1 to move in the undesired direction compared with the desired trajectory, and hence cable 2 requires a higher cable force to counteract this, as shown in Fig. 6(b). Since the motion is symmetrical about the XZ-plane, cables 4 and 5 behave similarly for the motion $t \ge 0.5$ s.

B. 8-Link 24-Degree of Freedom 8-Spherical Neck Model

To show the versatility and scalability of the generalized CRM formulation, a more complex 8-link example is presented. The kinematic structure is modeled to represent the human neck or cervical vertebrae, consisting of seven bones (bones C7–C1) and the skull. Links 1 to 7 represent bones C7 to C1, respectively, and link 8 represents the skull. As each joint possesses 3 DoFs, the total number of DoFs for the system is $n = 24$. The joints

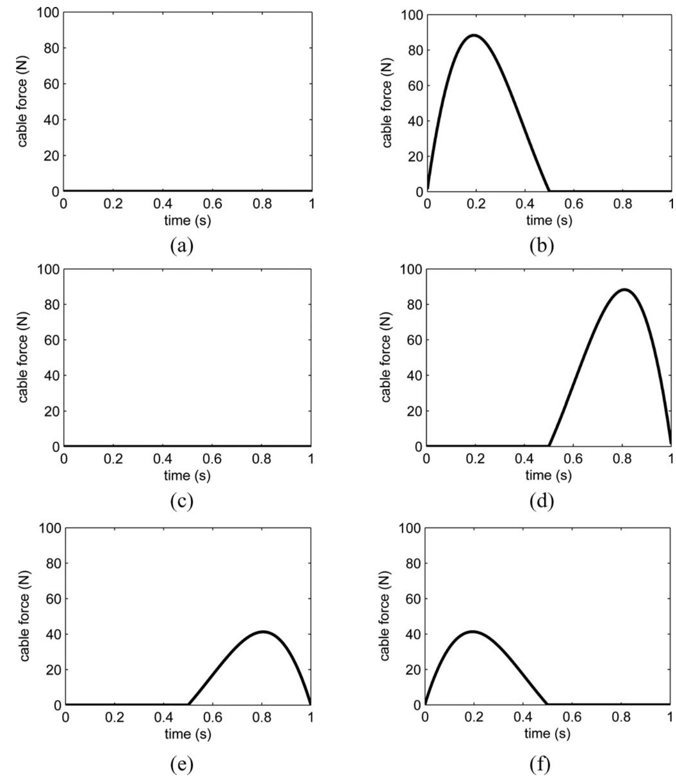

Fig. 6. Cable force profiles for 2-link SR trajectory. (a) Cable 1. (b) Cable 2. (c) Cable 3. (d) Cable 4. (e) Cable 5. (f) Cable 6.

between the bones of the system have been modeled as spherical (S) joints to approximate the cervical vertebrae joints.

The system consists of 76 cables, where the cable routing and attachment locations were obtained from a biomechanics model of the neck [35]. The muscles are symmetrically located such that 38 cables represent the left neck muscles and 38 cables are the right neck muscles. Fig. 7(a) shows the model from [35] visualized in the OpenSims software, and Fig. 7(b) shows the similarly structured cable-driven mechanism model constructed from the generalized CRM model.

The 8-link example demonstrates the simplicity in which arbitrary cable routing can be achieved for complex systems. The neck model consists of many different types of cable routing, from simple cableroutings consisting of a single segment to complex routings with multiple pass-through attachment points. For example, one of the neck muscles begin from the base of the neck (link 0) to the C5 bone (link 3), then the corresponding CRM for the cable model with the same routing can be expressed as

$$C_1 = \begin{bmatrix} -1 & 0 & 0 & 1 & 0 & 0 & 0 & 0 & 0 \\ 0 & 0 & 0 & 0 & 0 & 0 & 0 & 0 & 0 \\ \vdots & & & & & & & & \vdots \\ 0 & 0 & 0 & 0 & 0 & 0 & 0 & 0 & 0 \end{bmatrix}.$$

Considering a more complex example where the muscle begins from the C4 bone (link 4), then connects to bones C3 (link 5), C2 (link 6), C1 (link 7), and finally ends at the skull (link 8). The

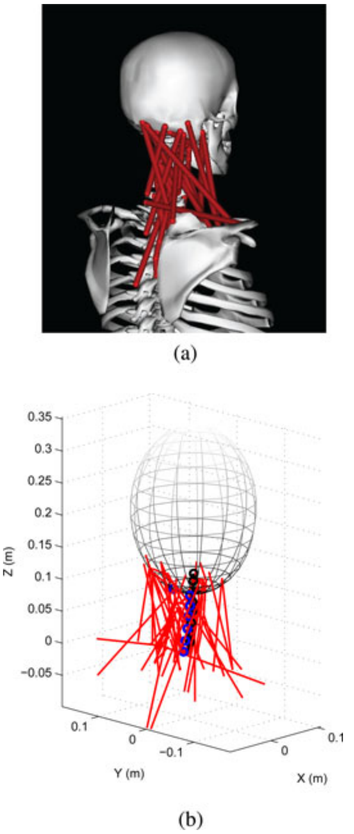

Fig. 7. 8-link 8-Spherical (8S) 76-cable model. Note that the proposed formulation is able to represent all of the muscle-routing from the OpenSim model. (a) OpenSim neck model. (b) 8-link 8S 76-cable model.

corresponding CRM for the cable model with the same routing can be expressed as

$$C_2 = \begin{bmatrix} 0 & 0 & 0 & 0 & -1 & 1 & 0 & 0 & 0 \\ 0 & 0 & 0 & 0 & 0 & -1 & 1 & 0 & 0 \\ 0 & 0 & 0 & 0 & 0 & 0 & -1 & 1 & 0 \\ 0 & 0 & 0 & 0 & 0 & 0 & 0 & -1 & 1 \\ 0 & 0 & 0 & 0 & 0 & 0 & 0 & 0 & 0 \\ \vdots & & & & & & & & \vdots \\ 0 & 0 & 0 & 0 & 0 & 0 & 0 & 0 & 0 \end{bmatrix}.$$

The aforementioned examples demonstrate the simplicity and flexibility of the proposed CRM representation for cable routing and the model of the system dynamics. After defining the CRM for specific cables, for example C_1 and C_2, the same generalized formulation presented in Sections IV and V can be utilized.

The generalized coordinates for the system can be represented by eight sets of Euler angles, where $\mathbf{q}_k = [\alpha_k \quad \beta_k \quad \gamma_k]^T$ are the xyz-Euler angles for joint k. Three simple trajectories were selected for the inverse dynamics simulation: roll motion $\mathbf{q}_{\text{roll}}(t)$, pitch motion $\mathbf{q}_{\text{pitch}}(t)$, and yaw motion $\mathbf{q}_{\text{yaw}}(t)$ that correspond to pure rotations in the X, Y, and Z axes, respectively. The roll, pitch, and yaw trajectories are generated by interpolating between initial and final generalized coordinates as shown in Table I. The initial and final velocities and accelerations for the generalized coordinates are zero, and the total time for each trajectory is 1 s.

The resulting force profiles for the roll, pitch, and yaw motion trajectories are shown in Figs. 8–10, respectively. Note that in this example muscles have been assumed to be ideal force generator elements [36]. For the roll trajectory $\mathbf{q}_{\text{roll}}(t)$, motion is purely in the YZ-plane and is symmetrical about the XZ-plane. Physically, this is analogous to the tilting of the head

TABLE I
TRAJECTORIES FOR 8-LINK 8S MODEL

Trajectory		Initial	Final
Roll Motion	$\mathbf{q}_1(t)$ - $\mathbf{q}_7(t)$	$(-\frac{\pi}{45}, 0, 0)$	$(\frac{\pi}{45}, 0, 0)$
	$\mathbf{q}_8(t)$	$(-\frac{\pi}{30}, 0, 0)$	$(\frac{\pi}{30}, 0, 0)$
Pitch Motion	$\mathbf{q}_1(t)$ - $\mathbf{q}_7(t)$	$(0, -\frac{\pi}{45}, 0)$	$(0, \frac{\pi}{45}, 0)$
	$\mathbf{q}_8(t)$	$(0, -\frac{\pi}{30}, 0)$	$(0, \frac{\pi}{30}, 0)$
Yaw Motion	$\mathbf{q}_1(t)$ - $\mathbf{q}_7(t)$	$(0, 0, -\frac{\pi}{45})$	$(0, 0, \frac{\pi}{45})$
	$\mathbf{q}_8(t)$	$(0, 0, -\frac{\pi}{30})$	$(0, 0, \frac{\pi}{30})$

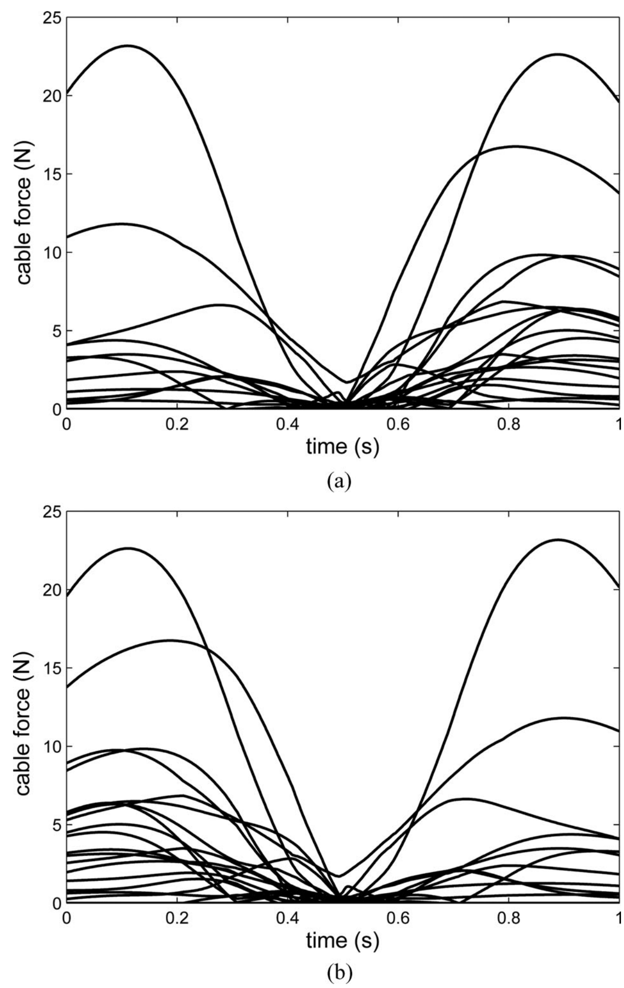

Fig. 8. Cables force profiles for the 8-Link 8S manipulator roll trajectory. (a) Cables forces (left muscles). (b) Cables forces (right muscles).

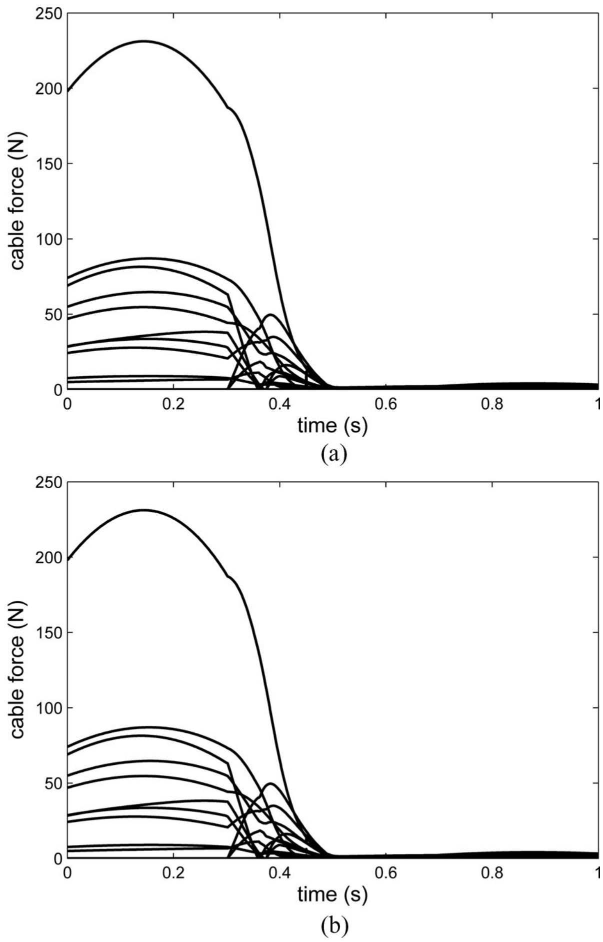

Fig. 9. Cables force profiles for the 8-Link 8S manipulator pitch trajectory. (a) Cables forces (left muscles). (b) Cables forces (right muscles).

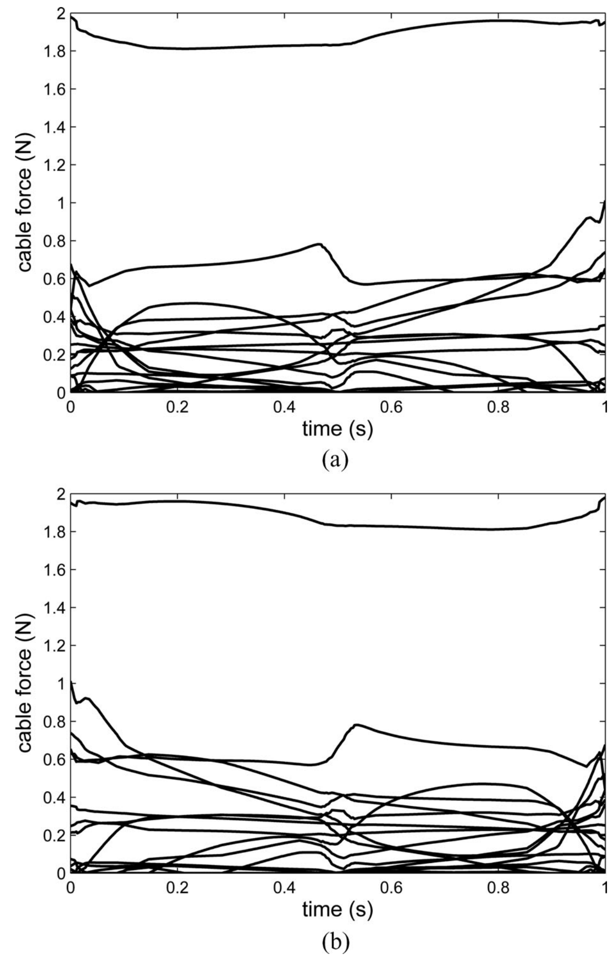

Fig. 10. Cables force profiles for the 8-Link 8S manipulator yaw trajectory. (a) Cables forces (left muscles). (b) Cables forces (right muscles).

from left to right. For this motion, it is expected that the left and right cables should be reflected about time $t = 0.5$ s. Fig. 8(a) and (b) shows the set of left and right cables, respectively, and reflection about $t = 0.5$ s can be observed. For this trajectory, the maximum cable force observed is approximately 23 N.

In comparison, $\mathbf{q}_{\text{pitch}}(t)$ motion is analogous to the tilting of the head from back to front. Since motion is in the XZ-plane, Fig. 9(a) and (b) shows that the corresponding left and right cables exert the same force for the entire trajectory. Furthermore, it can be observed that the first part of the motion $t < 0.5$ s requires a considerably larger amount of cable force, with a maximum of approximately 230 N, than the second half of the trajectory, with a maximum force of less than 10 N. This observation suggests that the cable attachment locations are arranged such that lower forces are required to operate in the positive XZ-plane. Similar to single link cable-driven systems, the performance and cable force characteristics heavily depend on the location of cable attachment locations. However, the performance of multilink cable-driven manipulators highly depends on both cable routing and attachment locations.

The effect of cable arrangement on manipulator's performance is further illustrated through the yaw motion $\mathbf{q}_{\text{yaw}}(t)$. The cable forces for the yaw trajectory for the left and right cables are shown in Fig. 10. The yaw motion is analogous to the panning motion of the head from right to left. Similar to the roll motion, it is expected that the set of left and right cable forces are reflected about time $t = 0.5$ s, as observed in Fig. 10(a) and (b). In comparison to the roll and pitch trajectories, it is apparent that the yaw motion requires the smallest cable force to perform, with a maximum cable force of approximately 2 N.

The 8-link model example demonstrates that the generalized model that is based on the CRM is able to describe the cable routing for complex systems, such as the routing of muscle within biomechanical systems. After formulating the generalized Jacobian matrix, analysis such as inverse dynamics, workspace analysis, and cable configuration optimization can be performed on the generalized system. Since the Jacobian matrix formulation is independent to the number of links, type of joints and cable routing, analysis can be formulated and performed for the generalized system.

VII. Conclusion and Future Work

A generalized model formulation for multilink open-chain cable-driven manipulators allowing arbitrary cable routing was presented. The CRM was introduced to encapsulate all possible routing of the cables for the system. The Jacobian matrix was derived with respect to the CRM through the formulation of the system kinematics and equations of motion. To demonstrate the versatility and advantages of the generalized system formulation, inverse dynamics analysis was performed on the generalized multilink manipulator model. This was simulated for two example manipulators: a simple 2-link 4-DoF 6-cable system and a more complex 8-link 24-DoF 76-cable system. Future work will focus on further applying analysis techniques on the generalized multilink manipulator model, such as workspace analysis, and extending these analysis techniques to study biomechanical systems due to their anthropomorphic similarities.

References

[1] S. Kawamura, W. Choe, S. Tanaka, and S. R. Pandian, "Development of an ultrahigh speed robot FALCON using wire drive system," in *Proc. IEEE Int. Conf. Rob. Autom.*, 1995, pp. 215–220.

[2] S. Kawamura, H. Kino, and C. Won, "High-speed manipulation by using parallel wire-driven robots," *Robotica*, vol. 18, pp. 13–21, 2000.

[3] J. S. Albus, R. V. Bostelman, and N. Dagalakis, "The NIST robocrane," *J. Robot. Sys.*, vol. 10, no. 5, pp. 709–724, 1993.

[4] S.-R. Oh, K. Mankala, S. K. Agrawal, and J. S. Albus, "A dual-stage planar cable robot: Dynamic modelling and design of a robust controller with positive inputs," *J. Mech. Des.*, vol. 127, pp. 612–620, 2005.

[5] P. H. Borgstrom, N. P. Borgstrom, M. J. Stealey, B. Jordan, G. S. Sukhatme, M. A. Batalin, and W. J. Kaiser, "Design and implementation of NIMS3D, a 3-D cabled robot for actuated sensing applications," *IEEE Trans. Robot.*, vol. 25, no. 2, pp. 325–339, Apr. 2009.

[6] R. L. Williams, II, J. S. Albus, and R. V. Bostelman, "3D cable-based cartesian metrology system," *J. Robot. Syst.*, vol. 21, no. 5, pp. 237–257, 2004.

[7] P. Bosscher, R. L. Williams, II, L. S. Bryson, and D. Castro-Lacouture, "Cable-suspended robotic contour crafting system," *Autom. Constr.*, vol. 17, pp. 45–55, 2007.

[8] F. Ferlay and F. Gosselin, "A new cable-actuated haptic interface design," in *Proc. Int. Conf. Hapt.: Percept., Devices, Scenarios*, 2008, pp. 474–483.

[9] G. Rauter, J. von Zitzewitz, A. Duschau-Wicke, H. Vallery, and R. Riener, "A tendon-based parallel robot applied to motor learning in sports," in *Proc. IEEE RAS EMBS Int. Conf. Biomed. Rob. Biomechatron.*, 2010, pp. 82–87.

[10] S. Perreault and C. M. Gosselin, "Cable-driven parallel mechanisms: Application to a locomotion interface," *J. Mech. Des.*, vol. 130, pp. 102301-1–102301-8, 2008

[11] Y. Mao and S. K. Agrawal, "Design of a cable-driven arm exoskeleton (CAREX) for neural rehabilitation," *IEEE Trans. Robot.*, vol. 28, no. 4, pp. 922–931, Aug. 2012.

[12] S. K. Agrawal, V. N. Dubey, J. J. Gangloff, Jr., E. Brackbill, Y. Mao, and V. Sangwan, "Design and optimization of a cable driven upper arm exoskeleton," *J. Med. Dev.*, vol. 3, pp. 031004-1–031004-8, 2009.

[13] A. Ming and T. Higuchi, "Study on multiple degrees-of-freedom positioning mechanism using wires— Part 1: Concept, design, and control," *Int. J. Jpn. Soc. Eng.*, vol. 28, no. 2, pp. 131–138, 1994.

[14] S. Fang, D. Franitza, M. Torlo, F. Bekes, and M. Hiller, "Motion control of a tendon-based parallel manipulator using optimal tension distribution," *IEEE/ASME Trans. Mechatronics*, vol. 9, no. 3, pp. 561–568, Sep. 2004.

[15] S.-R. Oh and S. K. Agrawal, "Cable suspended planar robots with redundant cables: Controllers with positive tensions," *IEEE Trans. Robot.*, vol. 21, no. 3, pp. 457–465, Jun. 2005.

[16] M. Hassan and A. Khajepour, "Optimization of actuator forces in cable-based parallel manipulators using convex analysis," *IEEE Trans. Robot.*, vol. 24, no. 3, pp. 736–740, Jun. 2008.

[17] S. Bouchard, C. Gosselin, and B. Moore, "On the ability of a cable-driven robot to generate a prescribed set of wrenches," *J. Mech. Rob.*, vol. 2, pp. 011010-1–011010-10, 2010.

[18] M. Hassan and A. Khajepour, "Analysis of bounded cable tensions in cable-actuated parallel manipulators," *IEEE Trans. Robot.*, vol. 27, no. 5, pp. 891–900, Oct. 2011.

[19] D. Lau, D. Oetomo, and S. K. Halgamuge, "Wrench-closure workspace generation for cable driven parallel manipulators using a hybrid analytical-numerical approach," *J. Mech. Des.*, vol. 133, pp. 071004-1–071004-7, 2011.

[20] W. B. Lim, G. Yang, S. H. Yeo, and S. K. Mustafa, "A generic force-closure analysis algorithm for cable-driven parallel manipulators," *Mech. Mach. Theory*, vol. 46, pp. 1265–1275, 2011.

[21] M. Gouttefarde, D. Daney, and J.-P. Merlet, "Interval-analysis-based determination of the wrench-feasible workspace of parallel cable-driven robots," *IEEE Trans. Robot.*, vol. 27, no. 1, pp. 1–13, Feb. 2011.

[22] D. Lau, K. Bhalerao, D. Oetomo, and S. K. Halgamuge, "On the task specific evaluation and optimisation of cable-driven manipulators," in *Advances in Reconfigurable Mechanisms and Robots I*, J. S. Dai, M. Zoppi, and X. Kong, Eds. London, U.K.: Springer-Verlag, 2012, ch. 63, pp. 707–716.

[23] M. J.-D. Otis, S. Perreault, T.-L. Nguyen-Dang, P. Lambert, M. Gouttefarde, D. Laurendeau, and C. Gosselin, "Determination and management of cable interferences bewteen two 6-dof foot platforms in a cable-driven locomotion interface," *IEEE Trans. Syst., Man, Cybern. A*, vol. 39, no. 3, pp. 528–544, May 2009.

[24] Y. Wischnitzer, N. Shvalb, and M. Shoham, "Wire-driven parallel robot: Permitting collisions between wires," *Int. J. Robot. Res.*, vol. 27, no. 9, pp. 1007–1026, 2008.

[25] S. Ma, S. Hirose, and H. Yoshinada, "CT ARM-I: Coupled tendon-driven manipulator model I-design and basic experiments," in *Proc. IEEE Int. Conf. Rob. Autom.*, 1992, pp. 2094–2100.

[26] J. K. Salisbury and J. J. Craig, "Articulated hands: Force control and kinematic issues," *Int. J. Robot. Res.*, vol. 1, no. 1, pp. 4–17, 1982.

[27] J. M. Inouye, J. J. Kutch, and F. J. Valero-Cuevas, "A novel synthesis of computational approaches enables optimization of grasp quality of tendon-driven hands," *IEEE Trans. Robot.*, vol. 28, no. 4, pp. 958–966, Aug. 2012.

[28] A. D. Deshpande, J. Ko, D. Fox, and Y. Matsuoka, "Control strategies for the index finger of a tendon-driven hand," *Int. J. Robot. Res.*, vol. 32, no. 1, pp. 115–128, 2013.

[29] S. Rezazadeh and S. Behzadipour, "Workspace analysis of multibody cable-driven mechanisms," *J. Mech. Rob.*, vol. 3, pp. 021005-1–021005-10, 2011.

[30] S. K. Mustafa and S. K. Agrawal, "On the force-closure analysis of n-DOF cable-driven open chains based on reciprocal screw theory," *IEEE Trans. Robot.*, vol. 28, no. 1, pp. 22–31, Feb. 2012.

[31] S. Rezazadeh and S. Behzadipour, "Tensionability conditions of a multibody system driven by cables," in *Proc. ASME Int. Mech. Eng. Congr. Expo.*, 2007, pp. 1369–1375.

[32] S. K. Mustafa and S. K. Agrawal, "Reciprocal screw-based force-closure of an n-DOF open chain: Minimum number of cables required to fully constrain it," in *Proc. IEEE Int. Conf. Rob. Autom.*, 2011, pp. 3029–3034.

[33] S. K. Mustafa, G. Yang, S. H. Yeo, W. Lin, and I.-M. Chen, "Self-calibration of a biologically inspired 7 DOF cable-driven robotic arm," *IEEE/ASME Trans. Mechatronics*, vol. 13, no. 1, pp. 66–75, Feb. 2008.

[34] P. H. Borgstrom, B. L. Jordan, G. S. Sukhatme, M. A. Batalin, and W. J. Kaiser, "Rapid computation of optimally safe tension distributions for parallel cable-driven robots," *IEEE Trans. Robot.*, vol. 25, no. 6, pp. 1271–1281, Dec. 2009.

[35] A. N. Vasavada, S. Li, and S. L. Delp, "Influence of muscle morphometry and moment arms on the moment-generating capacity of human neck muscles," *Spine*, vol. 23, no. 4, pp. 412–422, 1998.

[36] J. Yu, D. C. Ackland, and M. G. Pandy, "Shoulder muscle function depends on elbow joint position: An illustration of dynamic coupling in the upper limb," *J. Biomech.*, vol. 44, pp. 1859–1868, 2011.

Darwin Lau (M'12) received the B.Eng (Hons. 1) degree, in 2008, and the Ph.D. degree in mechanical engineering, robotics, in 2013, from the University of Melbourne, Parkville, Vic., Australia.

He joined the Department of Mechanical Engineering, the University of Melbourne, in May 2013, as a Research Fellow. His research interests include kinematics and dynamics of complex mechanisms, robotics, cable-driven parallel manipulators, and bioinspired mechanisms.

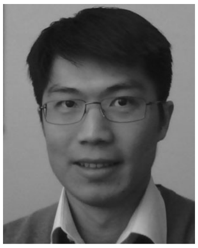

Denny Oetomo (SM'11) received the B.Eng (Hons. 1) degree from the Australian National University, Canberra, Australia, in 1997, and completed the Ph.D. degree (mechanical engineering, robotics) from the National University of Singapore, Singapore, in 2004.

He was a Research Fellow at the Department of Mechanical Engineering, Monash University, Melbourne, Australia from 2004–2006 and at INRIA Sophia-Antipolis (COPRIN), Sophia Antipolis, France from 2006–2007. He joined the Department of Mechanical Engineering, The University of Melbourne, Parkville, Vic., Australia, in January 2008, where he is currently a Senior Lecturer. His research interests include the area of kinematics, dynamics, and the effective control strategies of complex mechanisms.

Saman K. Halgamuge (SM'11) received the B.Sc. Eng. degree in electronic and telecommunication engineering from the University of Moratuwa, Moratuwa, Sri Lanka, in 1984, and the Dr.-Ing and Dipl.-Ing degrees from TU Darmstadt, Germany, in 1995 and 1990, respectively.

He is currently a Professor with the Department of Mechanical Engineering, University of Melbourne, Melbourne, Australia, where he is presently the Assistant Dean International of Melbourne School of Engineering. His research interests are in sensor networks, networked control, mechatronics, bioinformatics, bioinspired computing, and optimization algorithms.